Coordinate-Free Analysis of Mitral Valve Dynamics in Normal and Ischemic Hearts

Paul Dagum, MD, PhD; Tomasz A. Timek, MD; G. Randall Green, MD; David Lai, MD; George T. Daughters, MS; David H. Liang, MD, PhD; Motoya Hayase, MD; Neil B. Ingels, Jr, PhD; D. Craig Miller, MD

Background—The purpose of this investigation was to study mitral valve 3D geometry and dynamics by using a coordinate-free system in normal and ischemic hearts to gain mechanistic insight into normal valve function, valve dysfunction during ischemic mitral regurgitation (IMR), and the treatment effects of ring annuloplasty.

Methods and Results—Radiopaque markers were implanted in sheep: 9 in the ventricle, 1 on each papillary tip, 8 around the mitral annulus, and 1 on each leaflet edge midpoint. One group served as a control (n=7); all others underwent flexible Tailor partial (n=5) or Duran complete (n=6) ring annuloplasty. After an 8±2-day recovery, 3D marker coordinates were measured with biplane videofluoroscopy before and during posterolateral left ventricular ischemia, and MR was assessed by color Doppler echocardiography. Papillary to annular distances remained constant throughout the cardiac cycle in normal hearts, during ischemia, and after ring annuloplasty with either type of ring. Papillary to leaflet edge distances similarly remained constant throughout ejection. During ischemia, however, the absolute distances from the papillary tips to the annulus changed in a manner consistent with leaflet tethering, and IMR was observed. In contrast, during ischemia in either ring group, those distances did not change from preischemia, and no IMR was observed.

Conclusions—This analysis uncovered a simple pattern of relatively constant intracardiac distances that describes the 3D geometry and dynamics of the papillary tips and leaflet edges from the dynamic mitral annulus. Ischemia perturbed the papillary-annular distances, and IMR occurred. Either type of ring annuloplasty prevented such changes, preserved papillary-annular distances, and prevented IMR. **(*Circulation*. 2000;102[suppl III]:III-62-III-69.)**

Key Words: ischemia ■ regurgitation ■ mitral valve ■ valvuloplasty

Ischemic mitral regurgitation (IMR) remains a common and morbid clinical problem that continues to challenge cardiac surgeons. Because of the complexity of the mitral valve complex, many investigators have focused on isolated changes of specific substructures to begin to understand the factors that predispose to IMR. The proposed mechanisms range from theories of ischemia-induced deformation of the mitral annulus,[1,2] disturbances in papillary muscle dynamics,[3,4] and primary changes in LV shape and contractility[5–8] to theories that develop an integrated mechanism of LV contractility and mitral valve function[9,10] or of regional LV geometry and mitral valve function.[11–13] These disparate findings attest to our ignorance of this vexing problem.

The treatment of IMR remains as controversial as its mechanism.[14–16] Mitral valve repair is uniformly favored over mitral valve replacement in almost all mitral valve pathologies except IMR. Unlike structural MR, with its specific valvular anatomic pathological abnormalities, lack of a clear mechanistic understanding of IMR precludes a good understanding of how best to repair the valve. Traditional approaches have included ring annuloplasty, but the use of an annuloplasty ring has yielded mixed results.[17] More disturbing than the rather unpredictable results after ring annuloplasty repair has been the dearth in our ability to understand why ring annuloplasty sometimes works and at other times, fails.

Recent analyses of mitral valve function have used fixed or moving coordinate systems oriented with respect to certain mitral valve structures, such as the mitral annulus, to study the 3D geometry and dynamics of the mitral valve complex during the cardiac cycle.[11,12] Measurements of the 3D dynamic geometry of the mitral valve complex, however, depend on the choice of coordinate system. Subjectivity in the choice of coordinate system and the huge complexity inherent in processing and unifying the 3D coordinates of the mitral valve structures throughout the cardiac cycle may obfuscate salient findings and actually hinder our attempts to reach a mechanistic understanding of mitral valve function.

From the Department of Cardiovascular and Thoracic Surgery (P.D., T.A.T., G.R.G., D.L., G.T.D., N.B.I., D.C.M.) and the Division of Cardiovascular Medicine (D.H.L., M.H.), Stanford University School of Medicine, Stanford, and the Department of Cardiovascular Physiology and Biophysics (G.T.D., N.B.I.), Research Institute of the Palo Alto Medical Foundation, Palo Alto, Calif.

Correspondence to D. Craig Miller, MD, Department of Cardiovascular and Thoracic Surgery, Falk Cardiovascular Research Center, Stanford University School of Medicine, Stanford, CA 94305-5407. E-mail dcm@leland.stanford.edu

Circulation **is available at http://www.circulationaha.org**

To gain mechanistic insights into normal valve function and valve dysfunction during ischemia, we investigated mitral valve 3D geometry and dynamics in normal and ischemic hearts in a coordinate-free system that avoids the limitations imposed by coordinate-based analyses. To understand how ring annuloplasty may ameliorate IMR, we similarly analyzed the mitral valve in normal and ischemic hearts after 2 types of ring annuloplasty.

Methods

Sixteen adult, castrated male sheep were assigned to 3 experimental groups: a control group of sheep (no ring, n=7); a group that underwent Tailor flexible (partial, posterior) ring annuloplasty (Tailor [St. Jude Medical, Inc], size 31 mm, n=5); and a group that underwent Duran flexible (complete) ring annuloplasty (Duran [Medtronic Heart Valve Division], size 29 mm, n=2, and 31 mm, n=4). All 3 groups underwent identical surgical preparation, marker placement, and postoperative care. The details of the surgical preparation of the no-ring and Duran ring groups have been previously reported.[18]

Surgical Preparation

Nine miniature, radiopaque, tantalum markers (ID 0.8 mm, OD 1.3 mm, length 1.5 to 3.0 mm) were implanted on the LV epicardium through a left fifth intercostal space thoracotomy. The mitral and aortic valves were studied with epicardial echocardiography and color Doppler flow analysis. Cardiopulmonary bypass was instituted by using descending aorta and right atrial cannulation. Through a left atriotomy, 8 tantalum radiopaque markers were sutured ≈45° from 1 another around the circumference of the mitral annulus, and markers were sutured to each papillary muscle tip. The mitral valve was sized by using both the distance between the fibrous trigones and the area of the anterior leaflet, and the appropriate Tailor ring was sewn to the posterior annulus (trigone to trigone) with 8 to 10 interrupted, horizontal, mattress 2-0 Ethibond sutures. The animals were allowed to recover in the experimental animal cardiac surgical intensive care unit.

Experimental Design

After a recovery period (8±2 days [mean±SD]), the animals were premedicated with ketamine, intubated, and mechanically ventilated (veterinary anesthesia ventilator 2000, Hallowell EMC) with 100% oxygen. Transthoracic echocardiography with color Doppler was performed to assess proper seating of the annuloplasty ring and competence of the valve. Simultaneous biplane videofluoroscopic and hemodynamic data were acquired with the animal in the right lateral decubitus position. Animals were studied in normal sinus rhythm after autonomic blockade and with ventilation arrested at end expiration during data acquisition runs to minimize the effects of respiratory variation.

Lidocaine (1 mg/kg IV) was given, and a continuous infusion of lidocaine (1 mg/min) was started. An 8F Powerguide coronary guiding catheter (Advanced Cardiovascular Systems, Inc) was advanced into the left main coronary artery over a 0.014-in. Hi-Torque floppy guidewire (Advanced Cardiovascular Systems, Inc) through an 11F left carotid artery introducer. A conventional 3.5-mm nonperfusion balloon dilation catheter was advanced through the guiding catheter into the left circumflex artery (LCx) and positioned proximal to the second obtuse marginal branch. Control data were acquired before balloon inflation. The balloon was then inflated to 8 to 10 atm, and coronary angiography confirmed complete occlusion of the LCx. After 2 to 3 minutes of ischemia with the balloon inflated, data were again acquired, and MR was assessed by Doppler echocardiography.

All animals received humane care in compliance with the *Principals of Laboratory Animal Care* formulated by the National Society for Medical Research and the *Guide for Care and Use of Laboratory Animals* prepared by the National Academy of Sciences and published by the National Institutes of Health (DHEW[NIH] publication No. 85-23, revised 1985). This study was approved by the Stanford Medical Center Laboratory Research Animal Review Committee and conducted according to Stanford University policy.

Data Acquisition

A Philips Optimus 2000 biplane lateral ARC 2/poly Diagnost C2 system (Philips Medical Systems) was used to collect videofluoroscopic data at 60 Hz with the image intensifiers in the 9-in. mode. Two-dimensional images from each of the 2 x-ray views (45° right anterior oblique and 45° left anterior oblique) were digitized and merged to yield 3D coordinates for each radiopaque marker every 16.7 ms.[19] Analog left atrial, LV, and aortic pressures and ECG voltage were recorded on the video images during data acquisition and were simultaneously digitized with marker positions.

Data Analysis

End systole was defined as the videofluoroscopic frame preceding the maximum negative dP/dt ($-dP/dt_{max}$); end diastole was defined as the videofluoroscopic frame containing the peak of the ECG R-wave.

LV Systolic Function

Preload recruitable stroke work (PRSW), calculated from SW and end-diastolic volume (EDV), was used to assess global LV systolic function. An instantaneous estimate of LV volume was computed every 16.7 ms from the epicardial LV markers by using a multiple tetrahedral model reconstructed from the marker coordinates and corrected for LV convexity. Although epicardial LV volume calculated in this manner overestimates true LV chamber volume, the change in epicardial LV volume is an accurate measurement of the relative change in LV chamber volume.[20] Thus, stroke volume is accurately calculated from the change in epicardial LV volume, but ejection fraction (EF), or stroke volume normalized to epicardial LV end-diastolic volume, is substantially underestimated.

Mitral Valve Anatomic Locations

The key anatomic landmarks used in this study were the anterior and posterior commissures (ACOM and PCOM, respectively), the midlateral (midposterior) mitral annulus (lateral [posterior] annulus), the left and right fibrous trigones (LFT and RFT), the anterior and posterior papillary muscle tips (APT and PPT), and the centers of the free edge of the anterior mitral valve leaflet and the middle scallop of the posterior mitral valve leaflet (AMVL and PMVL, respectively) (Figure 1 and Table 1).

Mitral Annulus Geometry

Mitral annular dimensions were computed from the 3D marker coordinates. The commissure-commissure (CC) dimension was computed from the distance between the ACOM and PCOM markers, and the septal-lateral (SL) dimension was computed from the distance between the septal and lateral annular markers. Those distances were computed every 16.7 ms in the control data acquisition and during acute ischemia in all 3 groups.

Papillary Muscle Geometry

The position of each papillary muscle tip relative to the mitral annulus and mitral leaflets was computed from the 3D marker coordinates every 16.7 ms before and during acute ischemia in all 3 groups. The distances from each papillary muscle tip to 4 locations on the mitral annulus (ACOM, PCOM, posterior annulus, and either the LFT for the APT or the RFT for the PPT) and to each leaflet edge (AMVL and PMVL) were computed. Because distance measurements are independent of different choices of the 3D coordinate system, conclusions based on those distances are not confounded by the selection of any particular internal or external coordinate system.

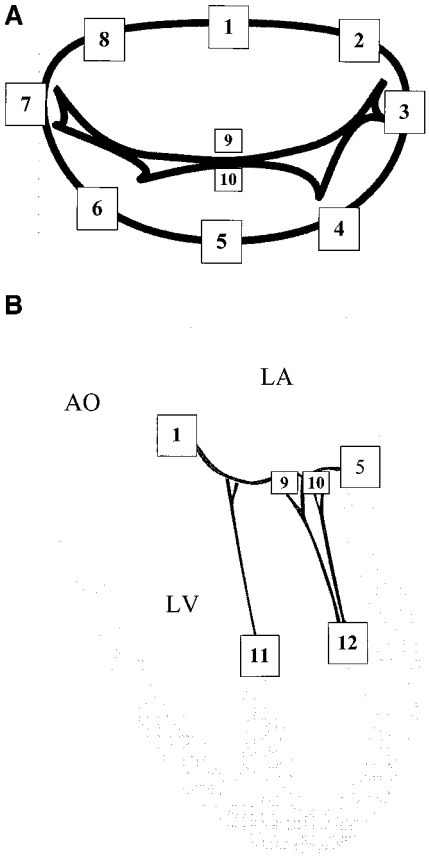

Figure 1. Miniature marker array used in this study. Eight markers were sutured circumferentially to mitral annulus at ≈45° from 1 another. These sites included midpoint between both fibrous trigones (marker 1), both fibrous trigones (markers 2 and 8), both commissures (markers 3 and 7), and midposterior annulus (marker 5, A). Markers were also sutured to free edge of anterior mitral leaflet (marker 9), free edge of middle cusp of posterior mitral leaflet (marker 10), and to each papillary muscle tip (markers 11 and 12, B). AO indicates aorta; LA, left atrium.

Statistical Analysis

All data are reported as mean±SD. For each animal, hemodynamic data represent the mean of 3 consecutive cardiac cycles. The papillary to annular distances represent distances measured at 16.7-ms intervals and averaged over all animals in each experimental group and those distances averaged throughout the cardiac cycle. Similarly, the papillary to leaflet distances represent distances measured at 16.7-ms intervals and averaged over all animals in each experimental group and those distances averaged throughout ejection. Comparisons were made with repeated-measures ANOVA, with the experimental group representing the nonrepeated factor and LCx ischemia representing the repeated factor. All reported probabilities were corrected for multiple comparisons (Bonferroni inequality correction). Significant changes with ischemia by repeated-measures ANOVA were resolved by the 2-tailed, paired Student's *t* test to identify the groups that changed significantly.

Results

Differences in body weight were not significant among the 3 groups (control 62±9 kg, Duran 69±8 kg, and Tailor 76±9 kg). Necropsy confirmed that all annuloplasty rings were seated properly. MR was not present by transthoracic color Doppler echocardiography in any animal at the time of control data acquisition.

TABLE 1. Mitral Valve Structures

Abbreviation	Structure
LFT	Left fibrous trigone
RFT	Right fibrous trigone
ACOM	Anterior commissure
PCOM	Posterior commissure
PA	Posterior annulus
AMVL	Anterior mitral valve leaflet
PMVL	Posterior mitral valve leaflet
APT	Anterior papillary tip
PPT	Posterior papillary tip
CC	Commissure-commissure
SL	Septal-lateral

Mitral Valve Regurgitation

Animals in all 3 groups had a competent mitral valve before acute LV ischemia. During ischemia, 2 animals in the no-ring group developed moderate to severe MR and the remaining 5 had mild to moderate MR. In the Tailor ring group, no animal developed MR with ischemia, and in the Duran ring group, 1 animal developed very slight MR.

Hemodynamics

Differences in heart rate, end-diastolic pressure, end-systolic pressure, EDV, end-systolic volume, stroke volume, EF, LV dP/dt_{max}, LV dP/dt_{min}, and PRSW were not significant across the 3 groups before or during ischemia (Table 2). Ischemia caused significant decreases in end-systolic pressure, EF, dP/dt_{max}, $-dP/dt_{min}$, and PRSW; a trend toward a decrease in EDV and stroke volume; and an increase in end-systolic volume, all of which are indicative of impaired LV systolic and diastolic function during ischemia.

Mitral Annulus

The CC and SL dimensions of the mitral annulus in the no-ring group underwent dynamic changes during the cardiac cycle, consistent with previously reported findings.[18] The CC and SL dimensions were largest during diastole (CC 37.0±2.0 mm and SL 28.0±1.2 mm) and at their minima during early systole (CC 33.7±1.4 mm and SL 24.3±1.2 mm; $P<0.001$ versus maximum for both). During ischemia, both mitral dimensions increased significantly ($P=0.001$ for both maximum and minimum SL versus control; $P=0.027$ for minimum CC versus control). These dimensions were again maximal during diastole (CC 37.0±2.0 mm and SL 30.3±1.8 mm) and smallest during systole (CC 34.6±1.7 mm and SL 27.4±1.8 mm; $P<0.001$ versus maximum during ischemia for both). Both the Tailor ring and the Duran ring annuloplasty eliminated CC and SL dynamic changes during the cardiac cycle (Figure 2). Furthermore, both rings prevented an increase in the CC dimension during ischemia, but only the complete Duran ring prevented an increase in the SL dimension (Tailor ring

TABLE 2. Hemodynamic Parameters Before and After Ischemia*

	Preischemia			Ischemia			ANOVA	
	No Ring	Tailor	Duran	No Ring	Tailor	Duran	P†	P‡
HR, bpm	106±10	119±14	114±10	102±19	97±35	96±32	NS	NS
EDP, mm Hg	16±4	20±10	25±9	20±5	23±4	23±8	NS	NS
ESP, mm Hg	98±24	94±12	102±13	74±17	67±19	76±23	NS	0.005
EDV, mL	145±33	173±25	198±43	149±37	181±26	197±42	NS	0.06
ESV, mL	115±23	141±17	159±27	125±26	154±15	165±32	NS	0.005
SV, mL	30±10	32±10	39±18	24±14	27±12	32±13	NS	0.09
EF, %	20±3	18±4	19±5	15±6	15±4	16±4	NS	0.01
dP/dt_{max}, mm Hg/s	2034±374	1534±430	1537±337	1565±321	1064±363	1156±345	NS	0.01
$-dP/dt_{min}$, mm Hg/s	1973±390	1627±308	1536±292	1432±372	1025±390	1068±433	NS	0.005
PRSW, mm Hg	69±19	63±11	55±13	56±15	43±11	42±14	NS	0.02

HR indicates heart rate; EDP, end-diastolic pressure; ESP, end-systolic pressure; ESV, end-systolic volume; and SV, stroke volume. Data are expressed as mean±SD.

*Ischemia was induced by 2 to 3 minutes of LCx occlusion.

Repeated-measures ANOVA probabilities are for nonrepeated factor (†experimental group) and repeated factor (‡ischemia). NS denotes $P>0.2$. All probabilities multiplied by 10 to correct for multiple comparisons (Bonferroni inequality correction).

preischemia SL 21.8±2.4 mm and ischemia SL 22.7±2.3 mm, $P=0.014$).

Anterior Papillary Muscle

Before LCx ischemia, the distances from the APT to the LFT, ACOM, and posterior annulus were relatively constant throughout the cardiac cycle in all 3 groups (Table 3). During ischemia, those distances also remained constant throughout the cardiac cycle, and in addition, no significant changes were observed in those distances before and during ischemia in either ring group (Figure 3). In the control group during ischemia, there was a small but highly significant increase in the distance between the APT and posterior annulus, a trend toward an increase in the distance between the APT and the LFT, and no significant changes in the distance between the APT and ACOM (Table 3). These results were surprising, most notably in the control group, because of the wide variations in the CC and SL dimensions found during the normal cardiac cycle and the large increase in both dimensions during ischemia (Figure 2). Furthermore, despite the significant annular size, shape, and dynamic distortions created by partial and complete flexible ring annuloplasty compared with the native annulus, the distances between the APT and its adjacent annulus (LFT, ACOM, and posterior annular) remained relatively constant throughout the cardiac cycle, both before and during ischemia.

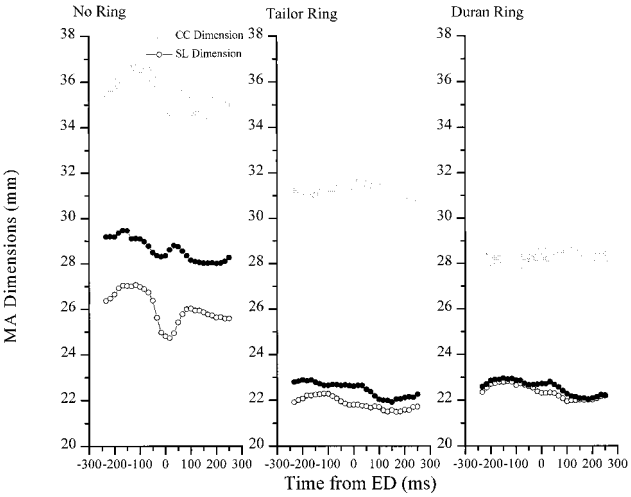

Figure 2. Mitral annular (MA) dimensions. CC and SL dimensions are shown in all 3 groups in control state (open symbols) and during acute ischemia (solid symbols). Each data point represents mean measurement over 3 complete cardiac cycles for all animals in respective groups. All cardiac cycles were aligned at end diastole (ED), and data points are 16.7 ms apart. Note dynamic changes in annular dimensions exhibited in no-ring group compared with absence of annular changes in both ring groups. This figure also displays dilating effect of acute ischemia on annular dimensions in no-ring group, whereas ischemia only increased SL dimension in Taylor ring group.

In contrast to the constant distances from the APT to the LFT, ACOM, and posterior annulus, the distance from the APT to the PCOM decreased during systole in all 3 groups in the control state. The distance was maximum near end diastole (no ring 40.1±2.4 mm; Tailor ring 40.2±2.7 mm; and Duran ring 36.9±1.9 mm) and minimum at end systole (no ring 35.8±2.0 mm, $P<0005$; Tailor ring 37.8±3.0 mm, $P=0.003$; and Duran ring 34.8±1.5 mm, $P<0.001$; respectively versus maximum).

Posterior Papillary Muscle

The geometric relationship between the posterior papillary muscle and its adjacent annulus (RFT, PCOM, and posterior annulus) was similar to the geometric relationship found between the anterior papillary muscle and mitral annulus. In all 3 groups, the distances from the PPT to the RFT, PCOM, and posterior annulus markers remained relatively constant throughout the cardiac cycle before ischemia and during ischemia (Figure 4). Again, no changes in any of the 3 distances before ischemia compared with the same distances during ischemia were observed in either ring group (Table 3). In the control group, however, the PPT to posterior annulus distance decreased significantly, and the PPT to RFT distance tended to increase during ischemia (Table 3). These changes in the PPT to annular

TABLE 3. Papillary-Annular and Papillary-Leaflet Distances*

	Preischemia			Ischemia			ANOVA	
	No Ring	Tailor	Duran	No Ring	Tailor	Duran	P†	P‡
APT-LFT	29.4±3.3	30.9±3.3	29.6±2.3	30.0±3.5	31.1±3.2	29.6±2.3	0.03	0.09
APT-ACOM	24.7±2.5	25.6±3.2	23.4±2.3	24.6±2.6	25.4±3.2	23.5±2.2	NS	NS
APT-PA	29.1±1.7	29.4±2.4	26.9±2.5	29.3±1.8	29.6±2.4	27.1±2.5	0.003	0.008
APT-AMVL	21.3±1.6	25.8±3.0	23.2±3.0	21.6±1.3	26.0±2.6	23.2±2.9	NS	NS
APT-PMVL	20.7±2.7	23.8±4.1	20.8±2.8	20.9±2.7	23.2±3.1	21.2±2.8	NS	NS
PPT-RFT	31.9±2.8	37.5±5.2	33.2±2.4	32.6±2.7	38.1±5.8	33.3±2.3	0.005	0.07
PPT-PCOM	27.4±2.1	30.6±4.5	26.0±2.5	27.3±2.0	30.4±4.9	25.6±2.4	NS	NS
PPT-PA	28.8±2.5	30.4±3.5	29.0±2.5	28.2±2.4	30.1±3.7	28.6±2.6	0.005	0.05
PPT-AMVL	21.6±1.1	26.0±2.8	24.9±2.9	22.0±0.8	26.5±2.9	25.0±2.8	NS	NS
PPT-PMVL	21.8±2.1	22.9±3.0	22.4±2.2	21.2±1.6	23.7±4.1	22.4±2.1	NS	NS

Data are expressed in mm as mean±SD.

*Ischemia was induced by 2 to 3 minutes of LCx occlusion.

Repeated-measures ANOVA probabilities for repeated factor (†ischemia) with nonrepeated factor (experimental group) were used to identify variables that differed significantly with ischemia while controlling for group. Two-tailed paired Student's *t* test was then used to identify the specific variables that differed. All tests between Tailor or Duran before and after ischemia were not significant except for APT-PMVL in the Tailor group ($P=0.027$).

‡Probabilities for the no-ring group are reported. NS denotes $P>0.2$. All probabilities are multiplied by 5 to correct for multiple comparisons (Bonferroni inequality correction).

geometry during ischemia suggest a corresponding displacement of the PPT toward the posterior annulus that coincided with the development of IMR in that group.

Even with the large distortions in the mitral annulus before and during ischemia in the control group, the distances between the APT and its adjacent annulus (LFT, ACOM, and posterior annulus) and between the PPT and its adjacent annulus (RFT, PCOM, and posterior annulus) were constant throughout the cardiac cycle before and during ischemia. Compared with preischemia values, the effect of ischemia was to alter these distances, which resulted in a displacement of the APT away from the posterior annulus and PPT toward it.

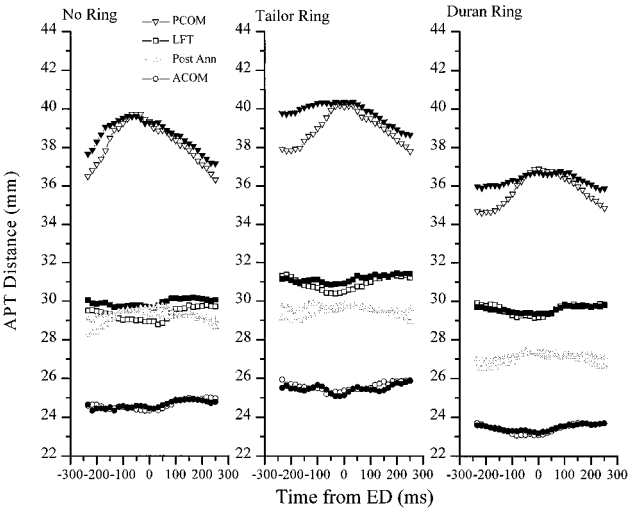

Figure 3. Anterior papillary–annular distances. Distances between APT and PCOM, LFT, posterior annulus (Post Ann), and ACOM are shown in all 3 groups in control state (open symbols) and during acute ischemia (solid symbols). Each data point represents mean measurement over 3 complete cardiac cycles for all animals in respective groups. All cardiac cycles were aligned at end diastole (ED), and data points are 16.7 ms apart. Distances from APT to LFT, ACOM, and posterior annulus were constant throughout cardiac cycle in all 3 groups and remained unchanged with ischemia in both ring groups.

Mitral Valve Leaflets

In all 3 experimental groups, the distances from each papillary tip to both the AMVL and the PMVL were constant

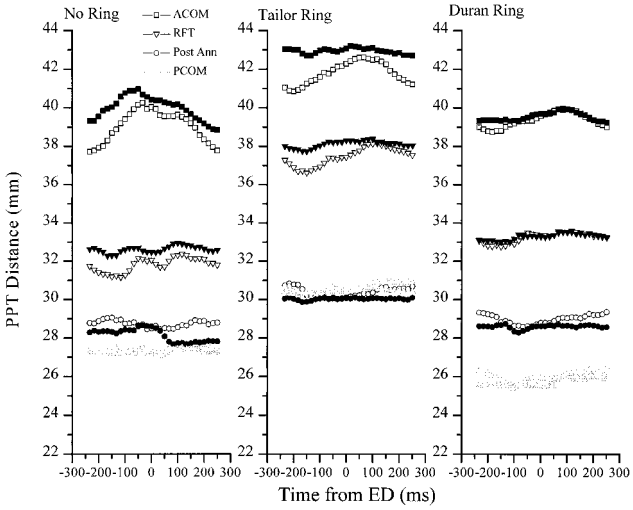

Figure 4. Posterior papillary–annular distances. Distances between PPT and ACOM, RFT, posterior annulus (Post Ann), and PCOM are shown in all 3 groups in control state (open symbols) and during acute ischemia (solid symbols). Each data point represents mean measurement over 3 complete cardiac cycles for all animals in respective groups. All cardiac cycles were aligned at end diastole (ED), and data points are 16.7 ms apart. In all 3 groups, distances from PPT to RFT, PCOM, and posterior annulus markers remained relatively constant throughout cardiac cycle before and during ischemia. Furthermore, no changes in any of 3 distances before ischemia compared with same distances during ischemia were observed in either ring group. In contrast to latter finding in both ring groups, significant changes were observed in no-ring group.

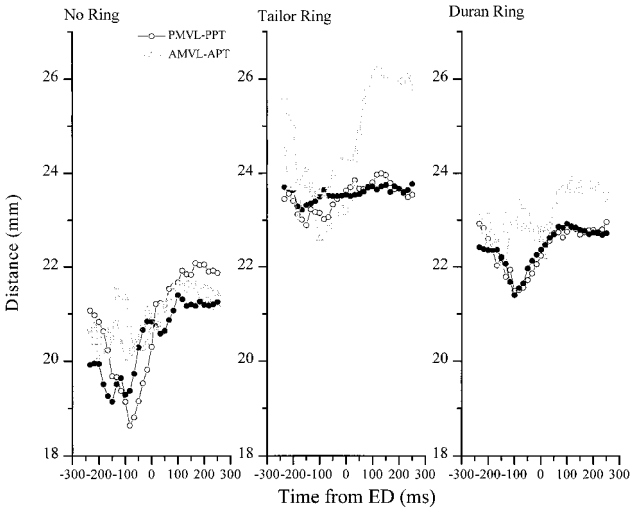

Figure 5. Papillary–leaflet edge distances. Distances between APT and AMVL and between PPT and PMVL are shown in all 3 groups in control state (open symbols) and during acute ischemia (solid symbols). Each data point represents mean measurement over 3 complete cardiac cycles for all animals in respective groups. All data were aligned at end diastole (ED), and data points are 16.7 ms apart. In all 3 experimental groups, distances from each papillary tip to both AMVL and PMVL were constant throughout LV ejection; during ischemia, those distances again remained constant. Thus, distances from papillary tips to leaflet midpoints remain constant, even after ischemic repositioning of papillary tips.

throughout LV ejection (Figure 5 and Table 3). During ischemia, those distances again remained constant; additionally, they did not differ significantly compared with their preischemia values, except for a small decrease in the APT to PMVL distance in the Tailor ring group (Table 3). These results are consistent with the notion that the chordae tendineae remain taut during ejection, and therefore, the distances from the papillary tips to the leaflet midpoints remain constant even after ischemic repositioning of the papillary tips.

Discussion

Conceptualizing the 3D geometry and motion of the mitral valve complex throughout the cardiac cycle is an unwieldy and difficult task. Prior analyses used a coordinate system representation of mitral valve structures.[11,12] To eliminate rigid-body rotation and translation artifacts, these coordinate systems must be fixed to a mitral valve structure, such as the mitral annulus. Different choices of coordinate system result in different geometry and dynamics that may mask important findings; this dilemma has precluded gaining more mechanistic insight into the coordinated function of the valvular and subvalvular structures.[11]

Using only distance measurements instead of a coordinate-based system, we found that a very simple pattern emerged from the complex dynamics of the mitral valve. In normal hearts, the papillary-annular distances (APT to LFT, ACOM, and posterior annulus; PPT to RFT, PCOM, and posterior annulus) remained relatively constant throughout the cardiac cycle, and the papillary–leaflet edge distances remained constant throughout ejection. Interestingly, this unvarying pattern of normal mitral valve motion was preserved when the valve was perturbed either by ischemia or by ring annuloplasty.

Although the constant pattern was preserved during ischemia, only the papillary–leaflet edge distances were identical before and during ischemia. With ischemia, the papillary-annular distances differed from preischemia, suggesting a repositioning of the papillary tips relative to the mitral annulus and hence, a change in the geometric relationship between the valvular and subvalvular structures. The APT distances to the LFT and posterior annulus increased, suggesting that it was displaced away from the annulus during ischemia. The PPT distance to the posterior annulus decreased, suggesting that it was displaced posteriorly during ischemia. Because the papillary–leaflet edge distances did not change with ischemia, these papillary tip displacements tethered the leaflets during systole, analogous to what Carpentier described as “type IIIb” restricted systolic leaflet motion in patients with IMR.

When the annulus was perturbed by using either a complete or partial ring annuloplasty, we again observed the simple pattern of constant papillary-annular and papillary–leaflet edge distances. As in the normal hearts with ischemia, we also found that after ring annuloplasty those distances again remained constant. Unlike the normal hearts with ischemia, however, in the ring groups with ischemia the papillary-annular distances did not differ from preischemia, and IMR was not observed.

A coordinate-free analysis of the mitral valve complex uncovered a simple pattern of constant distances that entirely describes the 3D geometry and dynamics of the papillary tips and leaflet edges from the dynamics of the mitral annulus. It is a well-known mathematical result that from the 3D positions of the mitral annular markers and each set of 3 papillary-annular distances we can uniquely determine the 3D position of each papillary tip. Because those distances were constant throughout the cardiac cycle, the 3D geometry of the mitral annulus at any point in the cardiac cycle governs the 3D position of the papillary tips. Furthermore, because the papillary–leaflet edge distances remained constant during ejection, the position and motion of the papillary tips also appeared to govern the 3D position and motion of the leaflet edges. These 2 results form the basis for the key conclusion from this analysis: The dynamic geometry of the mitral annulus determines the 3D position and motion of the leaflet edges during ejection.

In several clinical studies, annular dilation was the only mechanism of IMR identified in 25% to 50% of patients.[21–23] Although the latter group of patients would be categorized as having classic Carpentier type I (normal) leaflet motion, our findings suggest that the MR in these patients may be attributed partially to leaflet tethering, or type IIIb leaflet motion. Because of the intricate geometric relationships from annulus to papillary tips to leaflet edges, we cannot perturb in isolation the annulus, or the papillary tips, without affecting the other structures. This fact blurs the distinction between the Carpentier types of leaflet motion MR and also has important ramifications on the type of repair procedure used for the different types of leaflet motion encountered.

By abolishing normal annular dynamic motion,[20] annuloplasty rings also damp subvalvular dynamics. During acute ischemia, these rings prevent ischemic dilation of the annulus and therefore, prevent ischemic repositioning of the papillary tips and systolic tethering of the leaflets. Thus, at least in this animal model, ring annuloplasty would seem to be an effective surgical strategy for patients with IMR due to Carpentier type IIIb restrictive leaflet motion, in addition to those with traditional annular dilatation and normal (type I) leaflet motion.

The finding that the papillary-annular distances are constant was rather surprising. Those distances remained constant throughout the cardiac cycle during large changes in annular size and shape, after annular remodeling with a complete ring or posterior partial ring, and during acute ischemia that further accentuated changes in annular size and shape as well as caused significant changes in LV volumes and contractility. Regional annular distortions and size changes appear to displace the papillary tips in a predictable and quantifiable direction. Large asymmetric annular and ventricular deformations, however, lead to changes in the absolute distances, as was noted in the control group during ischemia. Because the papillary to leaflet edge distances must remain constant owing to the chordae tendineae, these perturbations unfavorably tether the leaflet edges apically during systole and predispose to IMR.

Many investigators studying the therapeutic mechanism of ring annuloplasty on IMR have explicitly discounted any potential effect of the procedure on the papillary muscles, as well as its indirect effects on the leaflets. The result of ring annuloplasty is generally dissociated from changes in subvalvular geometry and function. We reemphasize that an important corollary from the proposed mechanistic thesis supported by our findings is that any type of annular remodeling procedure will affect the subvalvular structures and therefore, will indirectly affect leaflet coaptation. The effect on those structures, specifically the position and dynamics of the papillary tips, is governed by the degree of annular distortion and dynamics. Furthermore, leaflet coaptation is governed by papillary tip position and dynamics and therefore, also by annular distortion and dynamics. Other models of functional MR, such as the MR observed in dilated cardiomyopathy (currently under investigation in our laboratory), may clarify further the role of these findings on the mechanism of MR. These physiologically relatively invariant distances between the mitral annulus and the subvalvular complex yield a simple mechanistic understanding that considerably facilitates the development of complex computer (finite-element analysis) models of the mitral valve designed to simulate various repair procedures in surgical planning for difficult mitral valve pathologies.[24]

Study Limitations

This experiment was performed in normal sheep hearts, which makes extrapolation to the clinical arena hazardous. Clinical IMR accompanies changes in LV contractility, size, and structure due to long-standing ischemia, infarction, or both, which are all associated with secondary changes in ventricular and papillary shape and geometry due to remodeling. Second, in this experiment, the ischemic insult was acute. Third, ring placement before the ischemic insult is distinctly different from the clinical situation, in which treatment follows the injury. Differences between human and ovine cardiac anatomy, especially in the area of the posterior annulus, have been described.[25] Although the rings were sized according to standard clinical criteria, reducing the orifice size of a normal mitral annulus differs from reducing the size of a mitral annulus that is already dilated secondary to long-standing MR. Last, changes in mitral complex dimensions before and after ischemia in the control group were small, but they were statistically significant and led to clinically significant MR.

Acknowledgments

This work was supported in part by grants HL-29589 and HL-48837 from the National Heart, Lung, and Blood Institute. Drs Dagum and Green were supported by National Heart, Lung, and Blood Institute Individual Research Service Awards HL10000-01 and HL-09569, respectively. Dr Timek is a recipient of the Thoracic Surgery Foundation Research Fellowship Award. Drs Dagum, Green, and Timek are Carl and Leah McConnell Cardiovascular Surgical Research Fellows. We appreciate the technical assistance provided by Mary K. Zasio, BA, Carol W. Mead, BA, and Erin K. Schultz, BS.

References

1. Glasson JR, Komeda M, Daughters GT, et al. Early systolic leaflet 'loitering' during acute ischemic mitral regurgitation. *J Thorac Cardiovasc Surg.* 1998;116:193–205.
2. Glasson JR, Komeda M, Daughters GT, et al. Three-dimensional dynamics of the canine mitral annulus during ischemic mitral regurgitation. *Ann Thorac Surg.* 1996;62:161–168.
3. Gorman JH III, Jackson BM, Gorman RC, et al. Papillary muscle discoordination rather than increased annular area facilitates mitral regurgitation after acute posterior myocardial infarction. *Circulation.* 1997; 96(suppl II):II-124–II-127.
4. Komeda M, Glasson JR, MacIsaac A, et al. Systolic 'dysfunction' of ischemic papillary muscle may serve as a compensatory mechanism for left ventricular wall motion abnormality. *Circulation.* 1995;92(suppl I):I-357. Abstract.
5. Van Dantzig JM, Delemarre BJ, Koster RW, et al. Pathogenesis of mitral regurgitation in acute myocardial infarction: importance of changes in left ventricular shape and regional function. *Am Heart J.* 1996;131:865–871.
6. Kaul S, Spotnitz WD, Glasheen WP, et al. Mechanism of ischemic mitral regurgitation: an experimental evaluation. *Circulation.* 1991;84: 2167–2180.
7. Kono T, Sabbah HN, Rosman H, et al. Left ventricular shape is the primary determinant of functional mitral regurgitation in heart failure. *J Am Coll Cardiol.* 1992;7:1594–1598.
8. Kono T, Sabbah, HN, Rosman H, et al. Mechanism of functional mitral regurgitation during acute myocardial ischemia. *J Am Coll Cardiol.* 1992;19:1101–1105.
9. Dent JM, Spotnitz WD, Nolan SP, et al. Mechanism of mitral leaflet excursion. *Am J Physiol.* 1995;69:H2100–H2108.
10. He S, Fontaine AA, Schwammenthal E, et al. Integrated mechanism for functional mitral regurgitation: leaflet restriction versus coapting force: in vitro studies. *Circulation.* 1997;96:1826–1834.
11. Komeda M, Glasson JR, Bolger AF, et al. Geometric determinants of ischemic mitral regurgitation. *Circulation.* 1997;96(suppl II):II-128–II-133.
12. Gorman RC, McCaughan JS, Ratcliffe MB, et al. Pathogenesis of acute ischemic mitral regurgitation in three dimensions. *J Thorac Cardiovasc Surg.* 1995;109:684–693.
13. Gorman JH III, Gorman RC, Jackson BM, et al. Distortions of the mitral valve in acute ischemic mitral regurgitation. *Ann Thorac Surg.* 1997;64: 1026–1031.

14. Cohn LH, Rizzo RJ, Adams DH, et al. The effect of pathophysiology on the surgical treatment of ischemic mitral regurgitation: operative and late risks of repair versus replacement. *Eur J Cardiothorac Surg.* 1995;9:568–574.
15. Akins CW, Hilgenberg AD, Buckley MJ, et al. Mitral valve reconstruction versus replacement for degenerative or ischemic mitral regurgitation. *Ann Thorac Surg.* 1994;58:668–675; Discussion 675–676.
16. Hendren WG, Nemec JJ, Lytle BW, et al. Mitral valve repair for ischemic mitral insufficiency. *Ann Thorac Surg.* 1991;52:1246–1251; Discussion 1251–1252.
17. David TE. Techniques and results of mitral valve repair for ischemic mitral regurgitation. *J Card Surg.* 1994;9(suppl):274–277.
18. Glasson JR, Green GR, Nistal JF, et al. Mitral annular size and shape in sheep with annuloplasty rings. *J Thorac Cardiovasc Surg.* 1999;117:302–309.
19. Niczyporuk MA, Miller DC. Automatic tracking and digitization of multiple radiopaque myocardial markers. *Comput Biomed Res.* 1991;24: 129–142.
20. Moon MR, DeAnda A, Daughters GT, et al. Experimental evaluation of different chordal preservation methods during mitral valve replacement. *Ann Thorac Surg.* 1994;58:931–944.
21. Dion R. Ischemic mitral regurgitation: when and how should it be corrected? *J Heart Valve Dis.* 1993;2:536–543.
22. Dion R, Benetis R, Elias B, et al. Mitral valve procedures in ischemic regurgitation. *J Heart Valve Dis.* 1995;4(suppl 2):S124–S129; Discussion S129–S131.
23. Hendren WG, Nemec JJ, Lytle BW, et al. Mitral valve repair for ischemic mitral insufficiency. *Ann Thorac Surg.* 1991;52:1246–1251; Discussion 1251–1252.
24. 23. Kunzelman KS, Reimink MS, Cochran RP. Flexible versus rigid ring annuloplasty for mitral valve annular dilation: a finite element model. *J Heart Valve Dis.* 1998;7:108–116.
25. Walmsley R. Anatomy of human mitral valve in adult cadaver and comparative anatomy of the valve. *Br Heart J.* 1978;40:351–366.

Coordinate-Free Analysis of Mitral Valve Dynamics in Normal and Ischemic Hearts

Paul Dagum, Tomasz A. Timek, G. Randall Green, David Lai, George T. Daughters, David H. Liang, Motoya Hayase, Neil B. Ingels, Jr and D. Craig Miller

Circulation. 2000;102:Iii-62-Iii-69
doi: 10.1161/01.CIR.102.suppl_3.III-62
Circulation is published by the American Heart Association, 7272 Greenville Avenue, Dallas, TX 75231

Print ISSN: 0009-7322. Online ISSN: 1524-4539